Composite Structures 111 (2014) 205–212

Contents lists available at ScienceDirect

Composite Structures

journal homepage: www.elsevier.com/locate/compstruct

# Static and dynamic of carbon nanotube reinforced functionally graded cylindrical panels

L.W. Zhang [a], Z.X. Lei [b,c], K.M. Liew [b,d,*], J.L. Yu [c]

[a] College of Information Technology, Shanghai Ocean University, 999 Huchenghuan Road, Shanghai 201306, PR China
[b] Department of Civil and Architectural Engineering, City University of Hong Kong, Kowloon, Hong Kong Special Administrative Region
[c] CAS Key Laboratory of Mechanical Behavior and Design of Materials, University of Science and Technology of China, PR China
[d] City University of Hong Kong Shenzhen Research Institute Building, Shenzhen Hi-Tech Industrial Park, Nanshan District, Shenzhen, PR China

ARTICLE INFO

*Article history:*
Available online 8 January 2014

*Keywords:*
Functionally graded materials
Ritz method
Shells
Vibration

ABSTRACT

The analysis of flexural strength and free vibration of carbon nanotube reinforced composite cylindrical panels is carried out. Four types of distributions of uniaxially aligned reinforcements are considered, i.e. uniform and three kinds of functionally graded distributions of carbon nanotubes along thickness direction of the panels. Material properties of nanocomposite panels are estimated by employing an equivalent continuum model based on the Eshelby–Mori–Tanaka approach. The governing equations are developed based on the first-order shear deformation shell theory. Detailed parametric studies have been carried out to reveal the influences of volume fraction of carbon nanotubes, edge-to-radius ratio and thickness on flexural strength and free vibration responses of the panels. In addition, effects of different boundary conditions and types of distributions of carbon nanotubes are examined.



## 1. Introduction

Recently, Carbon nanotubes (CNTs) have been widely accepted as a new advanced material with high strength and stiffness and a high aspect ratio and low density. Numerous investigators have reported remarkable physical and mechanical properties of this new form of carbon and CNTs may be selected as an excellent candidate for reinforcement of polymer composites. Sun et al. [1] analytically studied the axial Young's modulus of single-walled carbon nanotube arrays with diameters ranging from nanometer to meter scales. Their results confirmed that CNTs have mechanical properties superior than carbon fibers.

Researchers have analytically, experimentally and numerically investigated the constitutive models and mechanical properties of carbon nanotube polymer composites. Coleman et al. [2] reviewed and compared mechanical properties of single- and multi-walled carbon nanotube reinforced composites fabricated by various processes, in which the composites based on chemically modified nanotubes showed the best results since functionalization significantly enhances both dispersion and stress transfer. Tensile tests of CNT composites indicated that reinforcement with only 1 wt% nanotubes results in 36–42% increase in elastic modulus and 25% increase in breaking stress [3]. Odegard et al. [4] presented constitutive models of nanotubes-reinforced polymer composites with the nanotube, the local polymer near the nanotube and the nanotube/polymer interface modeled as effective continuum fibers, using an equivalent-continuum modeling method. By using molecular dynamic simulations, Griebel and Hamaekers [5] examined the elastic moduli of polymer-carbon nanotube composites with a single-walled carbon nanotube embedded in polyethylene. The results showed an excellent agreement with the macroscopic rule of mixtures. Based on the Mori–Tanaka effective-field method, Shi et al. [6] investigated effect of nanotube waviness and agglomeration on elastic properties of carbon nanotube reinforced composites.

Structure elements (beam, plate and shell) play an important role in actual structural applications. Carbon nanotube-reinforced composite (CNTRC) is an advanced material that can be embedded in beam, plate or shell as structural components. Bending behavior of one-dimensional structures is an important consideration in the design of structural components. Wuite and Adali [7] presented a multiscale analysis of deflection and stress behavior of symmetric cross-ply and angle-ply laminated CNTRC beams. Yas and Samadi [8] analysed free vibration and buckling of nanocomposite Timoshenko beams reinforced by single-walled carbon nanotubes (SWCNTs) resting on an elastic foundation using the generalized differential quadrature method. By employing an equivalent continuum model that follows the Eshelby–Mori–Tanaka approach, Formica et al. [9] studied vibration behaviors of CNTRC plates. Arani et al. [10] analytically and numerically investigated buckling behaviors of laminated composite plates in which optimal orientations of

* Corresponding author. Tel.: +852 34426581.
*E-mail address:* kmliew@cityu.edu.hk (K.M. Liew).

0263-8223/$ - see front matter © 2014 Elsevier Ltd. All rights reserved.
http://dx.doi.org/10.1016/j.compstruct.2013.12.035

CNTs required to achieve the highest critical load and the corresponding mode shapes were calculated for different kinds of boundary conditions, as well as aspect ratios of the plates. Motivated by the concept of functionally graded materials, some further investigations about functionally graded carbon nanotube reinforced composites (FG-CNTRC) have been conducted. With carbon nanotubes assumed graded in thickness direction of beams, Ke et al. [11] investigated nonlinear free vibrations of functionally graded nanocomposite beams. By using the mesh-free kp-Ritz, Lei et al. [12] analysed buckling of FG-CNTRC plates under various in-plane mechanical loads. Large deformation behaviors of FG-CNTRC plates were investigated in [13]. Wang and Shen [14] studied large amplitude vibration of FG-CNTRC plates resting on an elastic foundation in thermal environments. Aragh et al. [15] studied natural frequency characteristics of a continuously graded CNT-reinforced cylindrical panel, based on the Eshelby–Mori–Tanaka approach. For FG-CNTRC cylindrical shells, Shen and Xiang [16] examined the large amplitude vibration behavior of nanocomposite cylindrical shells in thermal environments. With FG-CNTRC cylindrical shells subject to axial compression and lateral pressure, postbuckling behaviors in thermal environments were analysed in [17,18].

The present work analyses flexural strength and free vibration of functionally graded carbon nanotube reinforced composite (FG-CNTRC) cylindrical panels. The mesh-free *kp*-Ritz method based on the first-order shear deformation shell theory is employed to derive the discretized governing equations. The CNTs are assumed to be uniaxially aligned in axial direction and functionally graded in thickness direction of the panels. The effective material properties of FG-CNTRC cylindrical panels are estimated through a micromechanical model based on the Eshelby–Mori–Tanaka approach. Several computational simulation examples are presented to figure out the effects of volume fraction of CNTs, edge-to-radius ratio, thickness, boundary conditions and distribution types of CNTs on flexural strength and free vibration responses of the panels.

## 2. Carbon nanotube reinforced composite panels

The configuration of the cylindrical panel considered in this paper is shown in Fig. 1. This panel is assumed to be thin and of length $L$, radius $R$, span angle $\theta_0$ and thickness $h$. As shown in Fig. 2, the CNTs are assumed to be uniaxially aligned in axial direction and functionally graded in thickness direction of the cylindrical panels, that is, UD is uniformly distributed; FG-V, FG-O and FG-X denote the other three types of functionally graded distributions of CNTs. For FG-V type panel, the top surface of the cylindrical panel is CNT-rich. For FG-O type panel, the middle surface of the cylindrical panel is CNT-rich and both top and bottom surfaces are CNT-rich for FG-X type panel. According to distributions of CNTs in the thickness direction of cylindrical panels, CNT volume fractions $V_{CNT}(z)$ are expressed as

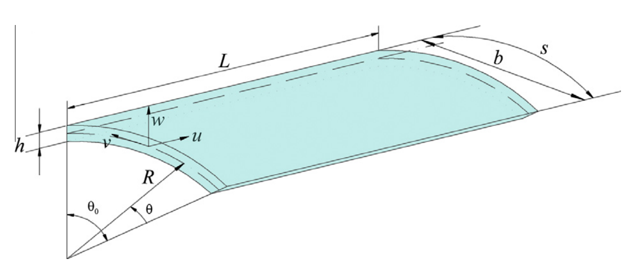


**Fig. 1.** Geometry properties of CNTRC panel.

$$V_{CNT}(z) = \begin{cases} V^*_{CNT} & \text{(UD)} \\ \left(1+\frac{2z}{h}\right)V^*_{CNT} & \text{(FG-V)} \\ 2\left(1-\frac{2|z|}{h}\right)V^*_{CNT} & \text{(FG-O)} \\ 2\left(\frac{2|z|}{h}\right)V^*_{CNT} & \text{(FG-X)} \end{cases}, \tag{1}$$

where

$$V^*_{CNT} = \frac{w_{CNT}}{w_{CNT} + (\rho^{CNT}/\rho^m) - (\rho^{CNT}/\rho^m)w_{CNT}}, \tag{2}$$

where $w_{CNT}$ is the fraction of mass of the CNTs, and $\rho^m$ and $\rho^{CNT}$ are densities of the matrix and CNTs, respectively.

Since the effective material properties of CNT-reinforced materials are sensitive to the structure of CNTs [19–22], several micromechanical models have been proposed to predict the effective material properties of CNT-reinforced nanocomposites, such as Eshelby–Mori–Tanaka scheme [9,23,24] and the extended rule of mixture [17,25,26]. According to Benveniste's revision [27], effective elastic module tensor $\mathbf{L}$ can be expressed as

$$\mathbf{L} = \mathbf{L}_m + V_{CNT}\langle(\mathbf{L}_{CNT} - \mathbf{L}_m)\cdot\mathbf{A}\rangle\cdot[V_m\mathbf{I} + V_{CNT}\langle\mathbf{A}\rangle]^{-1}, \tag{3}$$

where $\mathbf{I}$ is the fourth-order unit tensor and $\mathbf{L}_m$ and $\mathbf{L}_{CNT}$ are stiffness tensors of the matrix and CNT, respectively. The angle brackets represent an average over all possible orientation of the inclusions. $\mathbf{A}$ is the diluted mechanical strain concentration tensor and is written as

$$\mathbf{A} = \left[\mathbf{I} + \mathbf{S}\cdot\mathbf{L}_m^{-1}\cdot(\mathbf{L}_{CNT} - \mathbf{L}_m)\right]^{-1}, \tag{4}$$

where $\mathbf{S}$ is the fourth-order Eshelby tensor [28] and is well defined for cylindrical inclusions in [29].

## 3. Theoretical formulations

### 3.1. Displacement filed and strains of CNTRC panels

According to the first-order shear deformation shell theory [30], the displacement field is expressed as

$$u(x,\theta,z) = u_0(x,\theta) + z\phi_x(x,\theta), \tag{5}$$

$$v(x,\theta,z) = v_0(x,\theta) + z\phi_\theta(x,\theta), \tag{6}$$

$$w(x,\theta,z) = w_0(x,\theta), \tag{7}$$

where $(u_0, v_0, w_0, \phi_x, \phi_y)$ are displacement components at the middle surface of the panels ($z = 0$).

The strain–displacement equations are given as

$$\begin{Bmatrix} \varepsilon_{xx} \\ \varepsilon_{\theta\theta} \\ \gamma_{x\theta} \end{Bmatrix} = \boldsymbol{\varepsilon}_0 + z\boldsymbol{\kappa} = \begin{Bmatrix} \frac{\partial u_0}{\partial x} \\ \frac{1}{R}\frac{\partial v_0}{\partial \theta} + \frac{w_0}{R} \\ \frac{1}{R}\frac{\partial u_0}{\partial \theta} + \frac{\partial v_0}{\partial x} \end{Bmatrix} + z\begin{Bmatrix} \frac{\partial \phi_x}{\partial x} \\ \frac{1}{R}\frac{\partial \phi_\theta}{\partial \theta} \\ \frac{1}{R}\frac{\partial \phi_x}{\partial \theta} + \frac{\partial \phi_\theta}{\partial x} \end{Bmatrix}, \tag{8}$$

$$\begin{Bmatrix} \gamma_{yz} \\ \gamma_{xz} \end{Bmatrix} = \boldsymbol{\gamma}_0 = \begin{Bmatrix} \phi_\theta + \frac{1}{R}\frac{\partial w_0}{\partial \theta} - \frac{v_0}{R} \\ \phi_x + \frac{\partial w_0}{\partial x} \end{Bmatrix}. \tag{9}$$

### 3.2. Energy functional of analysis of flexural strength and free vibration of CNTRC cylindrical panels

For analysis of flexural strength, the panels are subjected to uniform transverse pressure loading $\mathbf{q}$, the strain energy of CNTRC cylindrical panels is given as

$$U_\varepsilon = \frac{1}{2}\int_0^L \int_0^{\theta_0} \boldsymbol{\varepsilon}^T\mathbf{S}\boldsymbol{\varepsilon}Rd\theta dx, \tag{10}$$

where

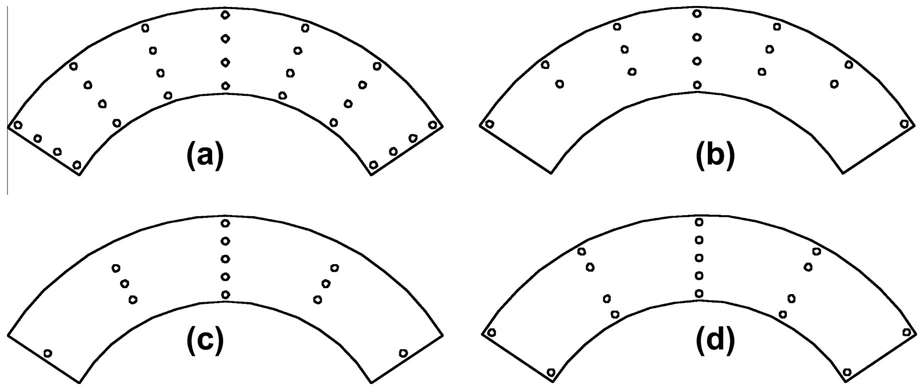


**Fig. 2.** Distribution types of CNTs of FG-CNTRC panels. (a) UD panel; (b) FG-V panel; (c) FG-O panel; and (d) FG-X panel.

$$\boldsymbol{\varepsilon} = \begin{Bmatrix} \boldsymbol{\varepsilon}_0 \\ \boldsymbol{\kappa} \\ \boldsymbol{\gamma}_0 \end{Bmatrix}, \tag{11}$$

$$\mathbf{S} = \begin{bmatrix} A_{11} & A_{12} & A_{16} & B_{11} & B_{12} & B_{16} & 0 & 0 \\ A_{12} & A_{22} & A_{26} & B_{12} & B_{22} & B_{26} & 0 & 0 \\ A_{16} & A_{26} & A_{66} & B_{16} & B_{26} & B_{66} & 0 & 0 \\ B_{11} & B_{12} & B_{16} & D_{11} & D_{12} & D_{16} & 0 & 0 \\ B_{12} & B_{22} & B_{26} & D_{12} & D_{22} & D_{26} & 0 & 0 \\ B_{16} & B_{26} & B_{66} & D_{16} & D_{26} & D_{66} & 0 & 0 \\ 0 & 0 & 0 & 0 & 0 & 0 & A^s_{44} & A^s_{45} \\ 0 & 0 & 0 & 0 & 0 & 0 & A^s_{45} & A^s_{55} \end{bmatrix} = \begin{bmatrix} \mathbf{A} & \overline{\mathbf{B}} & 0 \\ \overline{\mathbf{B}} & \mathbf{D} & 0 \\ 0 & 0 & \mathbf{A}_s \end{bmatrix}, \tag{12}$$

in which the extensional $A_{ij}$, coupling $B_{ij}$, bending $D_{ij}$ and transverse shear $A^s_{ij}$ stiffness are given by

$$(A_{ij}, B_{ij}, D_{ij}) = \int_{-h/2}^{h/2} Q_{ij}(1, z, z^2)dz, A^s_{ij} = K\int_{-h/2}^{h/2} Q_{ij}\,\mathrm{d}z. \tag{13}$$

The stiffness $A_{ij}$, $B_{ij}$ and $D_{ij}$ are defined for $i, j = 1, 2, 6$ whereas $A^s_{ij}$ is defined for $i, j = 4.5$. $K$ denotes the transverse shear correction coefficient, which can be computed such that the strain energy due to the transverse shear stresses equals the strain energy due to the true transverse stresses predicted by the 3-D elasticity theory. $Q_{ij}$ are the engineering constants related to the material properties, which are given as

$$Q_{11} = \frac{E_{11}}{1 - \upsilon_{12}\upsilon_{21}}, \quad Q_{22} = \frac{E_{22}}{1 - \upsilon_{12}\upsilon_{21}}, \quad Q_{12} = \frac{\upsilon_{21}E_{11}}{1 - \upsilon_{12}\upsilon_{21}}, \tag{14}$$

$$Q_{44} = G_{23}, \quad Q_{55} = G_{13}, \quad Q_{66} = G_{12}. \tag{15}$$

The external work due to uniform transverse pressure loading $\mathbf{q}$ is expressed as

$$W_e = \int_0^L \int_0^{\theta_0} \mathbf{u}^{\mathrm{T}}\mathbf{q}R\,\mathrm{d}\theta dx. \tag{16}$$

Thus the total potential energy functional of the panels for analysis of flexural strength is given by

$$\Pi_s = U_\varepsilon - W_e. \tag{17}$$

For analysis of free vibration, the panels are assumed to undergo a harmonic motion. The kinetic energy for the panels can be expressed as

$$\Theta = \frac{1}{2}\rho h \int_0^L \int_0^{\theta_0} (\dot{u}^2 + \dot{v}^2 + \dot{w}^2)R\,\mathrm{d}\theta dx. \tag{18}$$

Therefore, the total potential energy functional of the panels for analysis of free vibration is obtained as

$$\Pi_f = U_\varepsilon - \Theta. \tag{19}$$

### 3.3. Discrete system equations

For a cylindrical panel domain discretized by a set of nodes $\boldsymbol{x}_I$, $I = 1, \ldots, NP$, displacement approximations are expressed in the discrete form

$$\hat{\mathbf{u}} = \sum_{I=1}^{NP} \psi_I(x)\mathbf{u}_I, \tag{20}$$

where $\boldsymbol{u}_I$ is the nodal parameter and $\psi_I(x)$ is the shape function, defined as [31,32]

$$\psi_I(\boldsymbol{x}) = C(\boldsymbol{x}; \boldsymbol{x} - \boldsymbol{x}_I)\boldsymbol{\Phi}_a(x - x_I), \tag{21}$$

where $\Phi_a(\boldsymbol{x} - \boldsymbol{x}_I)$ is the kernel function and $C(\boldsymbol{x}; \boldsymbol{x} - \boldsymbol{x}_I)$ is the correction function which can be expressed by a linear combination of polynomial basis functions as

$$C(\boldsymbol{x}; \boldsymbol{x} - \boldsymbol{x}_I) = \mathbf{H}^{\mathrm{T}}(\boldsymbol{x} - \boldsymbol{x}_I)\mathbf{b}(\boldsymbol{x}) \tag{22}$$

$$\mathbf{b}(\boldsymbol{x}) = [b_0(\boldsymbol{x}, \theta), b_1(x, \theta), b_2(x, \theta), b_3(x, \theta), b_4(x, \theta), b_5(x, \theta)]^{\mathrm{T}}, \tag{23}$$

$$\mathbf{H}^{\mathrm{T}}(\boldsymbol{x} - \boldsymbol{x}_I) = \left[1, x - x_I, \theta - \theta_I, (x - x_I)(\theta - \theta_I), (x - x_I)^2, (\theta - \theta_I)^2\right]. \tag{24}$$

Thus, the shape function can be written as

$$\psi_I(\boldsymbol{x}) = \mathbf{b}^{\mathrm{T}}(\boldsymbol{x})\mathbf{H}(\boldsymbol{x} - \boldsymbol{x}_I)\Phi_a(\boldsymbol{x} - \boldsymbol{x}_I), \tag{25}$$

and Eq. (25) can be rewritten as

$$\psi_I(\boldsymbol{x}) = \mathbf{b}^{\mathrm{T}}(\boldsymbol{x})\mathbf{B}_I(\boldsymbol{x} - \boldsymbol{x}_I), \tag{26}$$

where

$$\mathbf{b}(\boldsymbol{x}) = \mathbf{M}^{-1}(\boldsymbol{x})\mathbf{H}(0), \tag{27}$$

$$\mathbf{B}_I(\boldsymbol{x} - \boldsymbol{x}_I) = \mathbf{H}(\boldsymbol{x} - \boldsymbol{x}_I)\Phi_a(\boldsymbol{x} - \boldsymbol{x}_I), \tag{28}$$

in which

$$\mathbf{M}(\boldsymbol{x}) = \sum_{I=1}^{NP} \mathbf{H}(\boldsymbol{x} - \boldsymbol{x}_I)\mathbf{H}^{\mathrm{T}}(\boldsymbol{x} - \boldsymbol{x}_I)\Phi_a(\boldsymbol{x} - \boldsymbol{x}_I), \tag{29}$$

$$\mathbf{H}(0) = [1, 0, 0, 0, 0, 0]^{\mathrm{T}}. \tag{30}$$

For the two-dimensional problem, the kernel function $\Phi_a(\boldsymbol{x} - \boldsymbol{x}_I)$ is defined as

$$\Phi_a(\boldsymbol{x}-\boldsymbol{x}_I)=\Phi_a(x)\cdot\Phi_a(\theta), \tag{31}$$

where

$$\Phi_a(x)=\varphi\left(\frac{\boldsymbol{x}-\boldsymbol{x}_I}{a}\right). \tag{32}$$

In the present study, the cubic spline function is selected as the weight function, and is given by

$$\varphi_z(z_I)=\begin{Bmatrix} \frac{2}{3}-4z_I^2+4z_I^3 & \text{for} 0\leqslant |z_I|\leqslant\frac{1}{2} \\ \frac{4}{3}-4z_I+4z_I^2-\frac{4}{3}z_I^3 & \text{for} \frac{1}{2}<|z_I|\leqslant 1 \\ 0 & \text{otherwise}\end{Bmatrix}, \tag{33}$$

where $z_I=\frac{x-x_I}{d_I}$ and $d_I$ is the size of the support of node $I$, calculated by

$$d_I=d_{\max}c_I, \tag{34}$$

where distance $c_I$ is chosen by searching for a sufficient number of nodes to avoid the singularity of matrix $\mathbf{M}$ and $d_{max}$ is a scaling factor ranging from 2.0 to 4.0.

Therefore, the shape function can be expressed as

$$\psi_I(\boldsymbol{x})=\mathbf{H}^{\mathrm{T}}(\mathbf{0})\mathbf{M}^{-1}(\boldsymbol{x})\mathbf{H}(\boldsymbol{x}-\boldsymbol{x}_I)\Phi_a(\boldsymbol{x}-\boldsymbol{x}_I) \tag{35}$$

Eq. (27) can be rewritten as

$$\mathbf{M}(\boldsymbol{x})\mathbf{b}(\boldsymbol{x})=\mathbf{H}(0). \tag{36}$$

The vector $\mathbf{b}(\boldsymbol{x})$ can be determined by using the LU decomposition of the matrix $\mathbf{M}(\boldsymbol{x})$, followed by the back substitution. Then by taking the first derivative of Eq. (35), we can obtain

$$\mathbf{M}_{,x}(\boldsymbol{x})\mathbf{b}(\boldsymbol{x})+\mathbf{M}(\boldsymbol{x})\mathbf{b}_{,x}(\boldsymbol{x})=\mathbf{H}_{,x}(0), \tag{37}$$

which can be rearranged as

$$\mathbf{M}(\boldsymbol{x})\mathbf{b}_{,x}(\boldsymbol{x})=\mathbf{H}_{,x}(0)-\mathbf{M}_{,x}(\boldsymbol{x})\mathbf{b}(\boldsymbol{x}). \tag{38}$$

It is noted that the first derivative of $\mathbf{b}(\boldsymbol{x})$ can be derived again using the LU decomposition procedure.

Thus, the first derivative of the shape function can be obtained by taking the derivative of Eq. (35), i.e.

$$\psi_{I,x}(\boldsymbol{x})=\mathbf{b}_{,x}^{\mathrm{T}}(\boldsymbol{x})B_I(\boldsymbol{x}-\boldsymbol{x}_I)+\mathbf{b}^{\mathrm{T}}(\boldsymbol{x})\mathbf{B}_{I,x}(\boldsymbol{x}-\boldsymbol{x}_I). \tag{39}$$

It is worth noting that the second derivative of the shape function can also be obtained by using the same procedure.

Since the shape function $\psi_I(\boldsymbol{x})$ does not possess Kronecker delta property, the essential boundary conditions cannot be directly imposed. In this paper, the transformation method is employed to impose the essential boundary conditions.

Based on the displacements defined in Eq. (20), $\tilde{u}$ is constructed as

$$\tilde{\mathbf{u}}_J=\hat{\mathbf{u}}(\boldsymbol{x}_J)=\sum_{I=1}^{NP}L_{IJ}\mathbf{u}_I, \tag{40}$$

where

$$L_{IJ}=\psi_I(x_J). \tag{41}$$

Eq. (40) can be rewritten as

$$\mathbf{u}_I=\sum_{I=1}^{NP}L_{IJ}^{-T}\tilde{\mathbf{u}}_I. \tag{42}$$

Substituting Eq. (42) into Eq. (40) leads to

$$\hat{\mathbf{u}}_J=\sum_{I=1}^{NP}\psi_I(x_J)\mathbf{u}_I=\sum_{I=1}^{NP}\sum_{K=1}^{NP}\psi_I(x)L_{KI}^{-T}\tilde{\mathbf{u}}_K=\sum_{K=1}^{NP}\hat{\psi}_K(x)\tilde{\mathbf{u}}_K, \tag{43}$$

where

$$\hat{\psi}_K(x)=\sum_{I=1}^{NP}L_{KI}^{-T}\psi_I(x), \tag{44}$$

Note that

$$\hat{\psi}_I(x_J)=\sum_{I=1}^{NP}L_{IK}^{-T}\psi_K(x_J)=\sum_{I=1}^{NP}L_{IK}^{-T}L_{kJ}=\delta_{IJ}. \tag{45}$$

Therefore, the reconstruction shape function possesses Kronecker delta property.

Substituting Eq. (20) into the total potential energy functional of analysis of flexural strength and free vibration of the panels and taking the variation of the total potential energy functional lead to the discrete system equations

$$\widetilde{\mathbf{K}}\mathbf{u}=\mathbf{F}, \tag{46}$$

$$(\widetilde{\mathbf{K}}-\omega^2\widetilde{\mathbf{M}})\mathbf{u}=0, \tag{47}$$

where

$$\widetilde{\mathbf{K}}=\mathbf{\Lambda}^{-1}\mathbf{K}\mathbf{\Lambda}^{-\mathrm{T}},\quad \mathbf{F}=\mathbf{\Lambda}^{-1}\mathbf{F},\quad \widetilde{\mathbf{M}}=\mathbf{\Lambda}^{-1}\overline{\mathbf{M}}\mathbf{\Lambda}^{-\mathrm{T}},\quad \tilde{\mathbf{u}}=\mathbf{\Lambda}\mathbf{u}. \tag{48}$$

Matrices $\mathbf{\Lambda}$, $\mathbf{K}$, $\mathbf{F}$, $\mathbf{M}$ and $\mathbf{u}$ are given as follows:

$$\Lambda_{IJ}=\psi_I(\boldsymbol{x}_J)\mathbf{I}, \mathbf{I}\text{ is the identity matrix} \tag{49}$$

$$\mathbf{u}=[u_1\ u_2\ \cdots\ u_n]^{\mathrm{T}}, \tag{50}$$

$$\mathbf{K}=\mathbf{K}^b+\mathbf{K}^m+\mathbf{K}^s, \tag{51}$$

$$\mathbf{K}_{IJ}^b=\int_0^L\int_0^{\theta_0}\left(\mathbf{B}_I^b\right)^{\mathrm{T}}\mathbf{D}\mathbf{B}_J^bR\,\mathrm{d}\theta\,\mathrm{d}x, \tag{52}$$

$$\mathbf{K}_{IJ}^m=\int_0^L\int_0^{\theta_0}(\mathbf{B}_I^m)^{\mathrm{T}}\mathbf{A}\mathbf{B}_J^mR\,\mathrm{d}\theta\,\mathrm{d}x+\int_0^L\int_0^{\theta_0}(\mathbf{B}_I^m)^{\mathrm{T}}\overline{\mathbf{B}}\mathbf{B}_J^bR\,\mathrm{d}\theta\,\mathrm{d}x+\int_0^L\int_0^{\theta_0}\left(\mathbf{B}_I^b\right)^{\mathrm{T}}\overline{\mathbf{B}}\mathbf{B}_J^mR\,\mathrm{d}\theta\,\mathrm{d}x, \tag{53}$$

$$\mathbf{K}_{IJ}^s=\int_0^L\int_0^{\theta_0}(\mathbf{B}_I^s)^{\mathrm{T}}\mathbf{A}^s\mathbf{B}_J^sR\,\mathrm{d}\theta\,\mathrm{d}x, \tag{54}$$

$$\overline{\mathbf{M}}=\int_{\mathbf{0}}^{\mathbf{L}}\int_{\mathbf{0}}^{\theta_{\mathbf{0}}}\mathbf{G}_{\mathbf{I}}^{\mathrm{T}}\bar{\mathbf{m}}\mathbf{G}_{\mathbf{J}}\mathbf{R}\,\mathbf{d}\theta\,\mathbf{dx}, \tag{55}$$

$$\mathbf{F}_I=\int_0^L\int_0^{\theta_0}\psi_I^T\mathbf{q}R\,\mathrm{d}\theta\,\mathrm{d}x, \tag{56}$$

where

$$\mathbf{B}_I^b=\begin{bmatrix}0&0&0&\frac{\partial\psi_I}{\partial x}&0\\0&0&0&0&\frac{1}{R}\frac{\partial\psi_I}{\partial\theta}\\0&0&0&\frac{1}{R}\frac{\partial\psi_I}{\partial\theta}&\frac{\partial\psi_I}{\partial x}\end{bmatrix}, \tag{57}$$

$$\mathbf{B}_I^m=\begin{bmatrix}\frac{\partial\psi_I}{\partial x}&0&0&0&0\\0&\frac{1}{R}\frac{\partial\psi_I}{\partial\theta}&\frac{\psi_I}{R}&0&0\\\frac{1}{R}\frac{\partial\psi_I}{\partial\theta}&\frac{\partial\psi_I}{\partial x}&0&0&0\end{bmatrix}, \tag{58}$$

$$\mathbf{B}_I^s=\begin{bmatrix}0&0&\frac{\partial\psi_I}{\partial x}&\psi_I&0\\0&-\frac{\psi_I}{R}&\frac{1}{R}\frac{\partial\psi_I}{\partial\theta}&0&\psi_I\end{bmatrix}, \tag{59}$$

$$\boldsymbol{\psi}_I^T = \begin{bmatrix} \psi_I & 0 & 0 & 0 & 0 \\ 0 & \psi_I & 0 & 0 & 0 \\ 0 & 0 & \psi_I & 0 & 0 \\ 0 & 0 & 0 & \psi_I & 0 \\ 0 & 0 & 0 & 0 & \psi_I \end{bmatrix}, \tag{60}$$

$$\bar{\mathbf{m}} = \begin{bmatrix} I_0 & 0 & 0 & I_1 & 0 \\ 0 & I_0 & 0 & 0 & I_1 \\ 0 & 0 & I_0 & 0 & 0 \\ I_1 & 0 & 0 & I_2 & 0 \\ 0 & I_1 & 0 & 0 & I_2 \end{bmatrix}, \tag{61}$$

where $I_0$, $I_1$ and $I_2$ are normal, coupled normal-rotary and rotary inertial coefficients, defined as

$$(I_0, I_1, I_2) = \int_{-2/h}^{h/2} \rho(z)(1, z, z^2)\,\mathrm{d}z. \tag{62}$$

To calculate the integrations for Eqs. (52)–(56), the stabilized nodal integration and direct nodal integration are employed, instead of Gauss integration, which may reduce computational cost and eliminate errors due to the mismatch between the quadrature cells and the shape function supports [33].

## 4. Numerical results

In this section, flexural strength and free vibration responses of FG-CNTRC cylindrical panels are investigated by using the mesh-free *kp*-Ritz method. Poly (methyl methacrylate), referred as PMMA, with material properties $\upsilon_m = 0.34$, $\alpha^m = 45(1 + 0.0005\Delta T) \times 10^{-6}$/K and $E^m = (3.52 - 0.0034T)$ GPa, where $T = T_0 + \Delta T$ and $T_0 = 300$ K (room temperature) is selected as the matrix. By using molecular dynamics simulations, Han and Elliott [34] obtained modulus of (10,10) SWCNTs ($E_{11}^{CNT} = 600$ GPa, $E_{22}^{CNT} = 10$ GPa, $G_{12}^{CNT} = 17.2$ GPa). The main cause of such a low value is that the effective thickness of CNTs is assumed as 0.34 nm. It is reported that the effective thickness of SWCNTs should be smaller than 0.142 nm and the effective wall thickness obtained for (10,10) SWCNTs is 0.067 nm, which satisfies the Vodenitcharova–Zhang criterion [35]. Thus the material properties used for the present study are selected from MD simulation results reported by Zhang and Shen [25]. For the present element-free method, a scaling factor of 3.1 that represents the size of the support is used for construction of shape functions and a regular nodal distribution 17 × 17 is chosen, following convergence studies.

### *4.1. Analysis of flexural strength of FG-CNTRC cylindrical panels*

Several numerical examples are provided for analysis of flexural strength of FG-CNTRC panels under mechanical loading. The effects of volume fraction of carbon nanotubes, edge-to-radius ratio, thickness, boundary conditions and distribution types of CNTs are examined in detail. Two kinds of boundary conditions, i.e. all edges simply supported and clamped, are considered. The boundary conditions are defined as

$$\begin{cases} x = 0, L : v_0 = w_0 = \phi_\theta = 0 \\ \theta = 0, \theta_0 : u_0 = w_0 = \phi_x = 0 \end{cases} \text{(Simply supported)}, \tag{63}$$

$$\begin{cases} x = 0, L : u_0 = v_0 = w_0 = \phi_x = \phi_\theta = 0 \\ \theta = 0, \theta_0 : u_0 = v_0 = w_0 = \phi_x = \phi_\theta = 0 \end{cases} \text{(Clamped)}. \tag{64}$$

To validate the present formulation, an analysis of isotropic cylindrical panel is carried out in terms of the number of nodes with different support sizes. Geometry and material properties of the panel are: $\theta_0 = 0.2$ rad, $R = 2.54$ m, $L/R = 0.2$, $h/R = 0.00125$, $E = 3.1$ Gpa, $\upsilon = 0.3$ and $q_0 = 275.8$ Pa. The boundary condition of the panel is four edges clamped. The central deflection (mm) is shown in Table 1. It can be seen that the present results agree well with other solutions available in the literature. According to the accuracy and efficiency, a discretization with 17 × 17 nodes and a scaling factor $d_{max} = 3.1$ are used for all further analyses.

Table 2 shows the non-dimensional central deflection $w/h$ of FG-CNTRC panels with different volume fractions of CNTs under uniformly distributed load $q_0 = 0.1$ MPa. The geometry of the panels is $\theta_0 = 0.1$ rad, $h = 0.002$ m, $h/R = 0.002$ and $L/R = 0.1$. It can be seen that the central deflection decreases with increase of volume fraction of CNTs. Since the constraint of clamped boundary condition is stronger than simply supported boundary condition, the central deflection of the panels with four edges simply supported is higher than that with four edges clamped. We can also observe that the central deflection for FG-O cylindrical panel has the highest value, while that of FG-X cylindrical panel is the lowest. Therefore, it is concluded that CNTs distributed close to top and bottom

**Table 1**
Central deflection (mm) of isotropic cylindrical panel under uniformly distributed loading.

| Nodes | $d_{max}$ | | | | Reddy [30] | Palazatto and Dennis [37] |
|---|---|---|---|---|---|---|
| | 2.2 | 2.5 | 2.8 | 3.1 | | |
| 9 × 9 | 0.2819 | 0.2831 | 0.2922 | 0.2954 | | |
| 11 × 11 | 0.2849 | 0.2842 | 0.2904 | 0.2919 | | |
| 13 × 13 | 0.2866 | 0.2854 | 0.2900 | 0.2914 | | |
| 15 × 15 | 0.2875 | 0.2861 | 0.2899 | 0.2908 | | |
| 17 × 17 | 0.2880 | 0.2865 | 0.2887 | 0.2905 | 0.288 | 0.289 |

**Table 2**
Non-dimensional central deflection $w/h$ of FG-CNTRC panels with different volume fractions of CNTs.

| | | $V_{CNT}$ | | | |
|---|---|---|---|---|---|
| | | 0.11 | 0.14 | 0.17 | 2.0 |
| SSSS | UD | 1.1156 | 0.8888 | 0.7270 | 0.6256 |
| | FG-V | 1.5515 | 1.2536 | 1.0171 | 0.8826 |
| | FG-O | 2.0221 | 1.6421 | 1.3287 | 1.1567 |
| | FG-X | 0.7708 | 0.6114 | 0.5009 | 0.4299 |
| CCCC | UD | 0.2500 | 0.2024 | 0.1625 | 0.1410 |
| | FG-V | 0.3482 | 0.2815 | 0.2281 | 0.1975 |
| | FG-O | 0.4477 | 0.3613 | 0.2935 | 0.2539 |
| | FG-X | 0.1800 | 0.1472 | 0.1165 | 0.1016 |

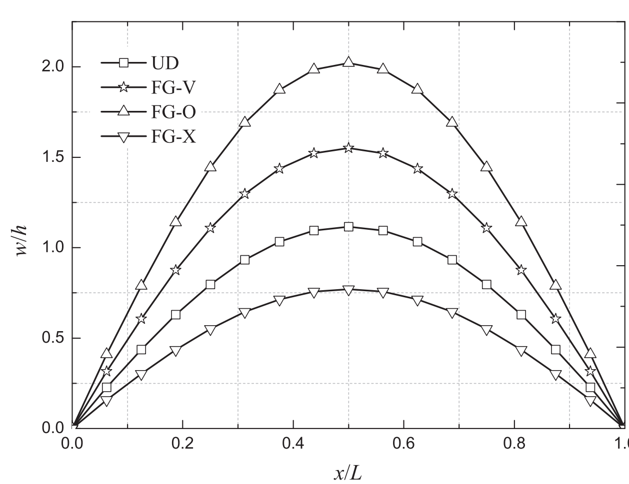

**Fig. 3.** Central deflection $w/h$ of FG-CNTRC panels along centerline $(x, \theta_0/2)$.

**Table 3**
Non-dimensional central deflection $w/h$ of FG-CNTRC panels for different edge-to-radius ratios ($L/R$).

| | | $L/R$ | | | | |
|---|---|---|---|---|---|---|
| | | 0.1 | 0.15 | 0.2 | 0.25 | 0.3 |
| SSSS | UD | 1.1156 | 4.8888 | 11.585 | 19.275 | 25.985 |
| | FG-V | 1.5515 | 6.1967 | 13.391 | 20.761 | 26.752 |
| | FG-O | 2.0221 | 7.8261 | 16.278 | 24.350 | 30.502 |
| | FG-X | 0.7708 | 3.5468 | 8.9446 | 15.797 | 22.318 |
| CCCC | UD | 0.2500 | 1.0878 | 2.4977 | 3.8725 | 4.8105 |
| | FG-V | 0.3482 | 1.4453 | 3.0325 | 4.3310 | 5.0786 |
| | FG-O | 0.3613 | 1.7831 | 3.5187 | 4.7848 | 5.4368 |
| | FG-X | 0.1016 | 0.7908 | 1.9349 | 3.2184 | 4.2268 |

**Table 4**
Non-dimensional central deflection $w/h$ of FG-CNTRC panels for different edge-to-radius ratios ($L/R$) with $h = 0.004$ m.

| | | $L/R$ | | | | |
|---|---|---|---|---|---|---|
| | | 0.1 | 0.15 | 0.2 | 0.25 | 0.3 |
| SSSS | UD | 0.0787 | 0.3307 | 0.7764 | 1.2834 | 1.7157 |
| | FG-V | 0.1073 | 0.4234 | 0.9166 | 1.4130 | 1.8001 |
| | FG-O | 0.1345 | 0.5293 | 1.1022 | 1.6374 | 2.0278 |
| | FG-X | 0.0567 | 0.2428 | 0.5995 | 1.0481 | 1.4679 |
| CCCC | UD | 0.0236 | 0.0854 | 0.1868 | 0.2917 | 0.3699 |
| | FG-V | 0.0297 | 0.1081 | 0.2240 | 0.3274 | 0.3939 |
| | FG-O | 0.0361 | 0.1310 | 0.2614 | 0.3674 | 0.4294 |
| | FG-X | 0.0191 | 0.0665 | 0.1485 | 0.2423 | 0.3210 |

**Table 5**
Comparison for the first six frequencies (Hz) for a clamped cylindrical panel.

| Mode | Node number | | | | Au and Cheung [36] |
|---|---|---|---|---|---|
| | $11 \times 11$ | $13 \times 13$ | $15 \times 15$ | $17 \times 17$ | |
| 1 | 881 | 874 | 869 | 867 | 869 |
| 2 | 939 | 944 | 951 | 956 | 957 |
| 3 | 1310 | 1300 | 1293 | 1291 | 1287 |
| 4 | 1387 | 1375 | 1367 | 1362 | 1363 |
| 5 | 1454 | 1444 | 1438 | 1435 | 1439 |
| 6 | 1714 | 1735 | 1740 | 1748 | 1751 |

**Table 6**
Non-dimensional frequency parameters $\bar{\omega} = \omega \frac{a^2}{h} \sqrt{\frac{\rho^m}{E^m}}$ of various FG-CNTRC panels with four edges simply supported and four edges clamped boundary conditions.

| | Mode | CNT distributions | | | |
|---|---|---|---|---|---|
| | | UD | FG-V | FG-O | FG-X |
| SSSS | 1 | 17.850 | 15.273 | 13.444 | 21.243 |
| | 2 | 22.073 | 20.183 | 18.482 | 25.096 |
| | 3 | 33.285 | 32.257 | 30.587 | 35.939 |
| | 4 | 51.778 | 51.410 | 48.702 | 54.535 |
| | 5 | 65.121 | 55.300 | 49.430 | 76.758 |
| | 6 | 67.264 | 58.006 | 51.505 | 78.556 |
| CCCC | 1 | 36.849 | 31.690 | 28.172 | 42.937 |
| | 2 | 40.924 | 36.567 | 33.213 | 46.640 |
| | 3 | 51.825 | 48.692 | 45.593 | 56.946 |
| | 4 | 70.638 | 68.671 | 65.505 | 75.394 |
| | 5 | 91.445 | 79.804 | 71.419 | 101.72 |
| | 6 | 93.611 | 82.583 | 74.350 | 104.00 |

surfaces are more efficient in increasing the stiffness of the cylindrical panels than CNTs distributed near the mid-surface.

**Table 7**
Non-dimensional frequency parameters $\bar{\omega} = \omega \frac{a^2}{h} \sqrt{\frac{\rho^m}{E^m}}$ of various FG-CNTRC panels with different thickness.

| $h$ | Mode | CNT distributions | | | |
|---|---|---|---|---|---|
| | | UD | FG-V | FG-O | FG-X |
| 0.004 | 1 | 23.773 | 14.524 | 12.888 | 19.618 |
| | 2 | 29.904 | 19.495 | 18.014 | 23.573 |
| | 3 | 45.691 | 31.329 | 29.863 | 34.331 |
| | 4 | 68.042 | 48.230 | 43.958 | 48.236 |
| | 5 | 68.158 | 48.313 | 46.677 | 48.317 |
| | 6 | 71.165 | 48.658 | 47.895 | 52.202 |
| 0.008 | 1 | 28.524 | 12.792 | 11.650 | 15.778 |
| | 2 | 37.405 | 17.645 | 16.635 | 19.867 |
| | 3 | 48.113 | 24.115 | 24.118 | 24.118 |
| | 4 | 48.195 | 24.156 | 24.158 | 24.158 |
| | 5 | 58.931 | 28.592 | 27.559 | 30.208 |
| | 6 | 75.339 | 35.430 | 33.503 | 39.486 |

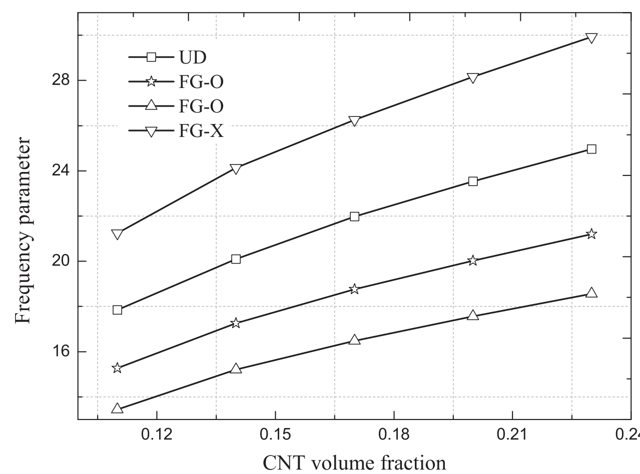


**Fig. 4.** Effect of volume fraction of CNTs on frequency parameters of FG-CNTRC panels with four edges simply supported boundary conditions.

Furthermore, the central deflection for the various types of FG-CNTRC panels along centerline $(x, \theta_0/2)$ is shown in Fig. 3.

Table 3 shows the non-dimensional central deflection $w/h$ of FG-CNTRC panels for different edge-to-radius ratios ($L/R$) with four edges simply supported and four edges clamped boundary conditions. It can be observed that the edge-to-radius ratio ($L/R$) has significant influence on the central deflection of the panels, as manifest in rapid increase of the central deflection caused when the edge-to-radius ratio ($L/R$) increases. A similar effect of the distribution types of CNTs in the panels is also observed with the change of edge-to-radius ratio ($L/R$). Subsequently, moderately thicker FG-CNTRC panels with $h = 0.004$ m are considered. Typical results are shown in Table 4. Some similar responses are obtained; the central deflections for thicker FG-CNTRC panels are relatively small.

### 4.2. Analysis of free vibration of FG-CNTRC cylindrical panels

The dynamic characteristics of various FG-CNTRC panels are presented in this section. Material and geometric properties are the same as those for analysis of flexural strength. Firstly, a comparative study is carried out for a clamped cylindrical panel. The panel has geometric properties as $h = 0.33$ mm, $L = 76.2$ mm, $\theta_0 = 0.133$ rad and $R = 762$ mm. Table 5 shows comparison of the present mesh-free results and solutions of Au and Cheung [36]

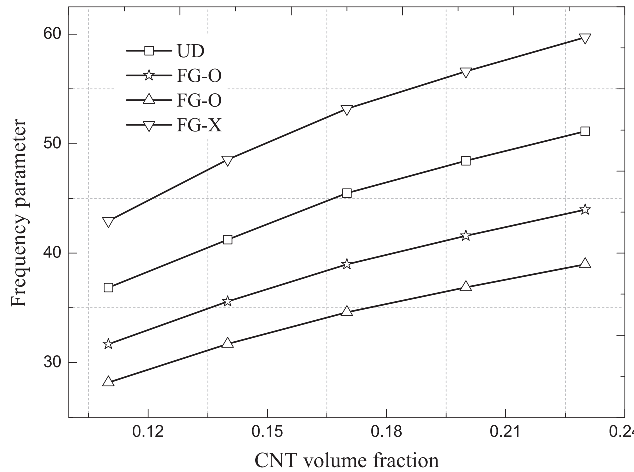


**Fig. 5.** Effect of volume fraction of CNTs on frequency parameters of FG-CNTRC panels with four edges clamped boundary conditions.

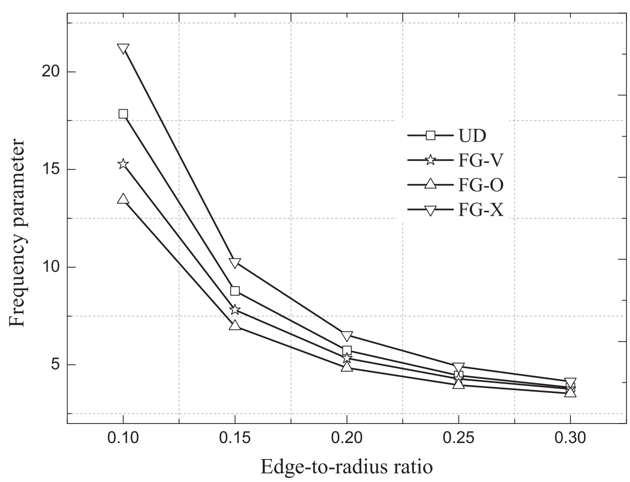


**Fig. 6.** Effect of edge-to-radius ratio ($L/R$) on frequency parameters of FG-CNTRC panels with four edges simply supported boundary conditions.

for first six frequencies, using isoparametric spline finite strip method. It can be seen that a good agreement is obtained.

Table 6 shows non-dimensional frequency parameters $\bar{\omega} = \omega \frac{a^2}{h}\sqrt{\frac{\rho^m}{E^m}}$ of various FG-CNTRC panels with four edges simply supported and four edges clamped boundary conditions. It can be seen that the frequency parameters of panels with four edges simply supported are lower than those of panels with four edges clamped. It is noted that FG-X panels have the highest frequency parameters and FG-O panels have the lowest frequency parameters among the panels. A further study is conducted to investigate the effect of thickness on frequency parameters of FG-CNTRC panels. Table 7 shows some similar observations.

Figs. 4 and 5 depict the effect of the volume fraction of CNTs on frequency parameters of FG-CNTRC panels with four edges simply supported and four edges clamped boundary conditions, respectively. It is found that frequency parameters of the panels have higher values when volume fraction of CNTs is higher since the stiffness of CNTRC panels is larger when the CNT volume fraction is higher. Compared with effect of volume fraction of CNTs, an opposite effect is observed for edge-to-radius ratio ($L/R$), as depicted in Figs. 6 and 7. It can be seen that frequency parameters decrease when the edge-to-radius ratios ($L/R$) increase. We can also observe that when the edge-to-radius ratio ($L/R$) increases from

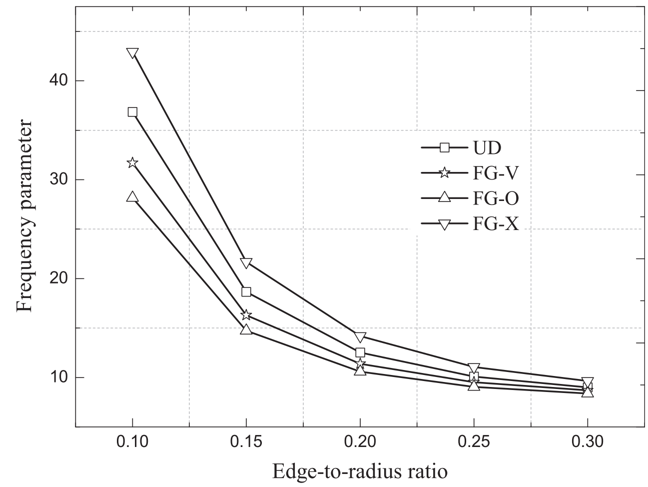


**Fig. 7.** Effect of edge-to-radius ratio ($L/R$) on frequency parameters of FG-CNTRC panels with four edges clamped boundary conditions.

0.1 to 0.3, at the beginning, the frequency parameters decrease quickly and the rate becomes gentler with further increase of the edge-to-radius ratio ($L/R$).

## 5. Conclusions

In this paper, the mesh-free *kp*-Ritz is employed for analysis of flexural strength and free vibration of functionally graded carbon nanotube-reinforced composite (FG-CNTRC) cylindrical panels. The formulations are based on the first-order shear deformation shell theory. The 2-D transverse displacement field is approximated by the mesh-free kernel particles estimate. The CNTs are assumed to be graded in thickness direction symmetric about the middle surface of the cylindrical panel and the effective material properties are estimated through a micromechanical model based on the Eshelby–Mori–Tanaka approach. Convergence and comparison studies are provided to assess the accuracy and efficiency of the present mesh-free method. Numerical examples are provided to present the static and dynamic characteristics of FG-CNTRC panels. Results reveal that volume fractions of carbon nanotubes, edge-to-radius ratios, thickness, boundary conditions and distribution type of CNTs have significant influences on the flexural strength and free vibration responses of the panels.

## References

[1] Sun CH, Li F, Cheng HM, Lu GQ. Axial Young's modulus prediction of single-walled carbon nanotube arrays with diameters from nanometer to meter scales. Appl Phys Lett 2005;87:193101–3.
[2] Coleman JN, Khan U, Blau WJ, Gun'ko YK. Small but strong: a review of the mechanical properties of carbon nanotube-polymer composites. Carbon 2006;44:1624–52.
[3] Qian D, Dickey EC, Andrews R, Rantell T. Load transfer and deformation mechanisms in carbon nanotube-polystyrene composites. Appl Phys Lett 2000;76:2868–70.
[4] Odegard GM, Gates TS, Wise KE, Park C, Siochi EJ. Constitutive modeling of nanotube-reinforced polymer composites. Compos Sci Technol 2003;63:1671–87.
[5] Griebel M, Hamaekers J. Molecular dynamics simulations of the elastic moduli of polymer-carbon nanotube composites. Comput Meth Appl Mech Eng 2004;193:1773–88.
[6] Shi DL, Feng XQ, Huang YY, Hwang KC, Gao HJ. The effect of nanotube waviness and agglomeration on the elastic property of carbon nanotube-reinforced composites. J Eng Mater Technol 2004;126:250–7.
[7] Wuite J, Adali S. Deflection and stress behaviour of nanocomposite reinforced beams using a multiscale analysis. Compos Struct 2005;71:388–96.
[8] Yas MH, Samadi N. Free vibrations and buckling analysis of carbon nanotube-reinforced composite Timoshenko beams on elastic foundation. Int J Pres Ves Pip 2012;98:119–28.

[9] Formica G, Lacarbonara W, Alessi R. Vibrations of carbon nanotube-reinforced composites. J Sound Vib 2010;329:1875–89.

[10] Arani A, Maghamikia S, Mohammadimehr M, Arefmanesh A. Buckling analysis of laminated composite rectangular plates reinforced by SWCNTs using analytical and finite element methods. J Mech Sci Technol 2011;25:809–20.

[11] Ke LL, Yang J, Kitipornchai S. Nonlinear free vibration of functionally graded carbon nanotube-reinforced composite beams. Compos Struct 2010;92:676–83.

[12] Lei ZX, Liew KM, Yu JL. Buckling analysis of functionally graded carbon nanotube-reinforced composite plates using the element-free kp-Ritz method. Compos Struct 2013;98:160–8.

[13] Lei ZX, Liew KM, Yu JL. Large deflection analysis of functionally graded carbon nanotube-reinforced composite plates by the element-free kp-Ritz method. Comput Meth Appl Mech Eng 2013;256:189–99.

[14] Wang ZX, Shen HS. Nonlinear vibration of nanotube-reinforced composite plates in thermal environments. Comput Mater Sci 2011;50:2319–30.

[15] Aragh BS, Barati AHN, Hedayati H. Eshelby–Mori–Tanaka approach for vibrational behavior of continuously graded carbon nanotube-reinforced cylindrical panels. Composites Part B 2012;43:1943–54.

[16] Shen HS, Xiang Y. Nonlinear vibration of nanotube-reinforced composite cylindrical shells in thermal environments. Comput Meth Appl Mech Eng 2012;213–216:196–205.

[17] Shen HS. Postbuckling of nanotube-reinforced composite cylindrical shells in thermal environments. Part I: axially-loaded shells. Compos Struct 2011;93:2096–108.

[18] Shen HS. Postbuckling of nanotube-reinforced composite cylindrical shells in thermal environments. Part II: pressure-loaded shells. Compos Struct 2011;93:2496–503.

[19] Li X, Gao H, Scrivens WA, Fei D, Xu X, Sutton MA, et al. Reinforcing mechanisms of single-walled carbon nanotube-reinforced polymer composites. J Nanosci Nanotechnol 2007;7:2309–17.

[20] Esawi AMK, Farag MM. Carbon nanotube reinforced composites: potential and current challenges. Mater Des 2007;28:2394–401.

[21] Seidel GD, Lagoudas DC. Micromechanical analysis of the effective elastic properties of carbon nanotube reinforced composites. Mech Mater 2006;38:884–907.

[22] Anumandla V, Gibson RF. A comprehensive closed form micromechanics model for estimating the elastic modulus of nanotube-reinforced composites. Composites Part A 2006;37:2178–85.

[23] Sobhani Aragh B, Nasrollah Barati AH, Hedayati H. Eshelby–Mori–Tanaka approach for vibrational behavior of continuously graded carbon nanotube-reinforced cylindrical panels. Composites Part B 2012;43:1943–54.

[24] Wang J, Pyrz R. Prediction of the overall moduli of layered silicate-reinforced nanocomposites-part I: basic theory and formulas. Compos Sci Technol 2004;64:925–34.

[25] Shen HS, Zhang CL. Thermal buckling and postbuckling behavior of functionally graded carbon nanotube-reinforced composite plates. Mater Des 2010;31:3403–11.

[26] Shen HS. Nonlinear bending of functionally graded carbon nanotube-reinforced composite plates in thermal environments. Compos Struct 2009;91:9–19.

[27] Benveniste Y. A new approach to the application of Mori–Tanaka's theory in composite materials. Mech Mater 1987;6:147–57.

[28] Eshelby JD. The determination of the elastic field of an ellipsoidal inclusion, and related problems. Proc R Soc Lond Ser A 1957;241:376–96.

[29] Mura T. Micromechanics of defects in solids. 2nd ed. The Netherlands: Martinus Nijhoff; 1987.

[30] Reddy JN. Mechanics of laminated composite plates and shells: theory and analysis. 2nd ed. Boca Raton, FL: CRC Press; 2004.

[31] Chen JS, Pan C, Wu CT, Liu WK. Reproducing Kernel Particle Methods for large deformation analysis of non-linear structures. Comput Meth Appl Mech Eng 1996;139:195–227.

[32] Liu WK, Jun S, Zhang YF. Reproducing kernel particle methods. Int J Numer Meth Fluids 1995;20:1081–106.

[33] Beissel S, Belytschko T. Nodal integration of the element-free Galerkin method. Comput Meth Appl Mech Eng 1996;139:49–74.

[34] Han Y, Elliott J. Molecular dynamics simulations of the elastic properties of polymer/carbon nanotube composites. Comput Mater Sci 2007;39:315–23.

[35] Wang CY, Zhang LC. A critical assessment of the elastic properties and effective wall thickness of single-walled carbon nanotubes. Nanotechnology 2008;19:075075.

[36] Au FTK, Cheung YK. Free vibration and stability analysis of shells by the isoparametric spline finite strip method. Thin-Wall Struct 1996;24:53–82.

[37] Palazotto AN, Dennis ST. Nonlinear analysis of shell structures. Washington, DC: AIAA; 1992.